ADVANCED FUNCTIONAL MATERIALS
www.afm-journal.de

Polyoxometalate-Modified Sponge-Like Graphene Oxide Monolith with High Proton-Conducting Performance

Yiwei Liu, Shumei Liu, Xuying Lai, Jun Miao, Danfeng He, Ning Li, Fang Luo, Zhan Shi, and Shuxia Liu**

Graphene oxide (GO) contains abundant oxygen-containing functional groups acting as hydrogen bond acceptors for proton conduction on its basal plane. However, the dilemma in realizing bulk in-plane conduction and the metastability at room temperature of GO films both obstruct its application. Polyoxometalate-modified sponge-like GO monolith (PEGO) with 3D cross-linking inner structure, which exhibits unique "shrink-expand" effect to polar solvent, are synthesized. Owing to the introduction of polyoxometalates and the replacement of unstable epoxy groups by ethylenediamine, PEGO exhibits hitherto the highest proton conductivity under low relative humidity (1.02×10^{-2} S cm^{-1} at 60% relative humidity) and excellent long-term stability (more than 1 month). The outstanding conductivity originates from 3D transporting pathways, high-density hopping sites, and eliminated grain boundary resistance. This study provides a practical way to design GO-based proton-conducting material dominated by in-plane diffusion.

1. Introduction

Graphene oxide (GO) has attracted considerable attention from researchers as one of the main precursors of graphene-based materials. Although the exact structure of GO has not been determined, epoxy, hydroxyl, and carboxyl groups are widely accepted as the main functional groups on both its 2D basal planes and edges,[1] which endow it with various technological applications.[2–4] Recently, the proton-conducting properties of GO-based materials were reported.[5–8] The protolysis process is proposed occurring through hydrogen-bonding networks constructed by the oxygen-containing functional groups and water molecules attached on the surface through a Grotthuss mechanism. In all of these reports, two assembly methods have been used for conductivity measurement. The first was compressing powder sample into a pellet, in which the GO fragments stacked randomly. The disordered arrangement will restrain protons moving when they are perpendicular to the proton transfer path (Figure S1a, Supporting Information). The other was GO papers/films obtained by vacuum filtration of colloidal dispersions of GO sheets.[2] In the laminated structure, the movement of protons through the bulk papers/films occur along the edges and pinholes of GO sheets with negligible in-plane conduction (Figure S1b, Supporting Information). Owing to the anisotropic conductivity for GO, videlicet, the through-plane conductivity is much lower than that in the in-plane direction,[7,8] both of the two assembly ways are suboptimal. Realizing proton conduction dominated by in-plane diffusion in a practical way has great significance. Besides that, GO films are metastable at room temperature. Epoxide groups, which have been proved as the major contributor for the in-plane journey of protons, are deprived within a relaxation time of about 1 month,[9] cutting off the hydrogen-bonding networks and accordingly blocking proton movement. Hence, substituting more stable hopping sites for epoxide groups in the interlayer of GO sheets is also important.

Polyoxometalates (POMs) are a huge family of inorganic metal–oxygen clusters on nanometer scale. Solid POMs possess a discrete ionic structure, comprising fairly mobile basic structural units heteropolyanions and countercations (H^+, H_3O^+, $H_5O_2^+$, etc.) This unique structure manifests itself to exhibit an extremely high proton mobility.[10–12] In 1979, Nakamura and co-workers first reported the proton conductivity of phosphotungstic acid ($H_3PW_{12}O_{40}\cdot 28H_2O$, HPW) which is comparable to 2 M phosphoric acid aqueous solution.[13] This high conductivity and potential application attracted widespread attention.[14] However, POMs are water-soluble and have poor machinability; they must be anchored on stable matrix to form practical materials.[15–18] Until recently, only a few polyoxometalate–graphene composites were reported.[19–24] In these materials, the oxygen-containing groups on GO basal plane are almost completely reduced, which is a disadvantage for proton conduction. In order to get high proton conductivity, it is necessary to introduce POMs into the interlayer space of GO sheets on the premise of retaining proton hopping sites as far as possible. The key challenge is that POMs can hardly be steady anchored on pristine GO directly owing to the

Y. Liu, Dr. S. Liu, X. Lai, J. Miao, D. He, N. Li, Prof. F. Luo, Prof. S. Liu
Key Laboratory of Polyoxometalate Science of the Ministry of Education
College of Chemistry
Northeast Normal University
Changchun, Jilin 130024, P. R. China
E-mail: luof746@nenu.edu.cn; liusx@nenu.edu.cn
Prof. Z. Shi
State Key Laboratory of Inorganic Synthesis and Preparative Chemistry
College of Chemistry
Jilin University
Changchun, Jilin 130012, P. R. China

DOI: 10.1002/adfm.201501912

© 2015 WILEY-VCH Verlag GmbH & Co. KGaA, Weinheim

electrostatic repulsion between the electronegative oxygen-containing groups and polyanions. Based on the above-mentioned considerations, we chose a weak reductant, ethylenediamine (EN) with flexible chain structure and amino hydrogen bond acceptor to selectively replace the unstable epoxide groups and obtained a sponge-like monolith with 3D cross-linking inner structure. POMs were introduced into the porous scaffold by simple soaking. The combination of rich oxygen sites, delocalized hydrogen ions, outstanding hydrophilicity, and 3D continuous pathways led to a proton conductivity of 1.02×10^{-2} S cm^{-1} at 60% relative humidity (RH), which is the highest under low RH and is comparable to that of the reported GO-based materials at nearly 100% RH.

2. Results and Discussion

The POMs-modified GO (PEGO) monolith material is synthesized by a two step process (**Figure 1**). First, EN was grafted on the basal plane of GO through ring-opening reaction between the pre-existing epoxy groups on GO basal plane and amino groups of EN.[25,26] A spontaneous assembly occurred during the reacting process. GO colloidal dispersion tardily agglomerated into a monolith cross-linked by EN molecules (**Figure 2**). In this way, we got an EN-functionalized GO (EGO). Then POMs were introduced into the interlayer of EGO sheets by impregnation. HPW has the strongest acidity, approaching the superacid region, among the common Keggin-type POMs, and ball-like profile with a diameter of about 1 nm.[11] There

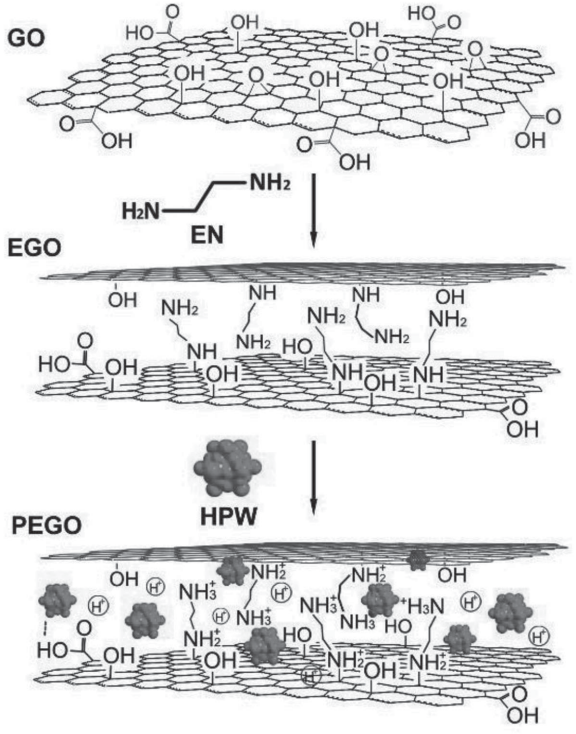

Figure 1. Illustration of the synthesis process of PEGO. GO was premodified by EN and the hydroxyl and carboxylic groups were retained. Then HPW were introduced into the interlayers by immersion.

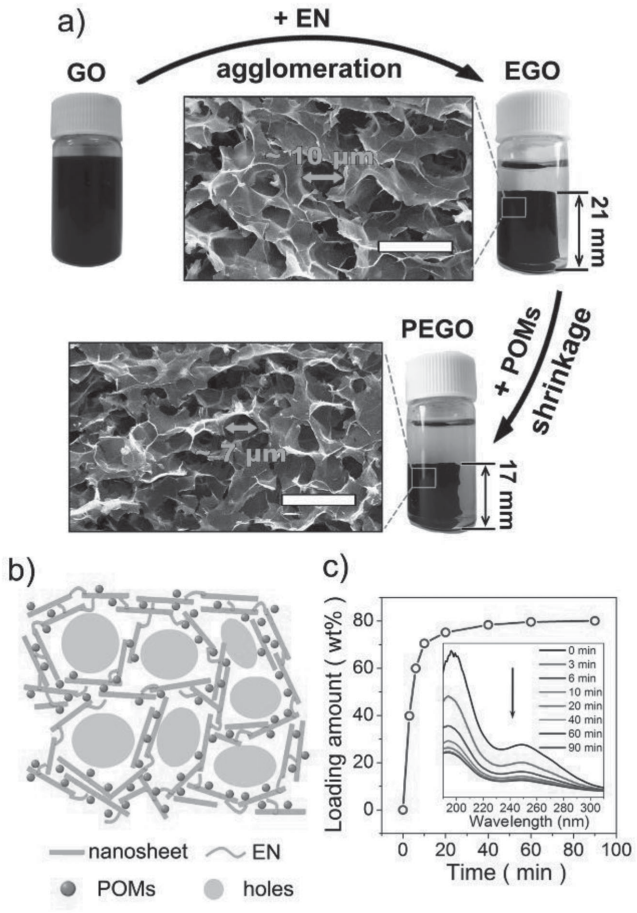

Figure 2. a) Digital images of the morphology change during the fabrication process of PEGO monolith and SEM images of the inner structure of EGO and PEGO monolith (scale bar 20 μm). b) The schematic of cross-linking inner structure of PEGO mediated by EN and POMs molecules. c) The loading amount of HPW on EGO over time. Inset: UV–vis spectrum of POMs aqueous solution which were soaked with EGO sampled periodically.

are three protons per HPW unit and these protons can dissociate from heteropolyanions in aqueous solution. As a result, the HPW unit is negatively charged in water. When EGO was soaked in HPW aqueous solution, the amino groups were protonated and positively charged under acid condition. Thus, HPW molecules/clusters would be assembled into the interlayer of EGO sheets by electrostatic attraction. Interestingly, an obvious shrinkage was observed with a dramatic volume decrease along with the injection of HPW (Figure 2a). This phenomenon might be attributed to the strong electrostatic attraction between polyanions and protonated EN, which narrowed the inner space of the cross-linked EGO sheets and further enhanced their connection, proved by the decreased pore size in scanning electron microscope (SEM) images (Figure 2a). In order to obtain the loading amount of HPW in the PEGO, UV–vis spectrum was used to monitor the adsorption process. A rapid adsorption equilibrium achieved within 20 min with an unprecedented high POMs loading capacity of about 80 wt% (Figure 2c). The high loading of POMs suggested a potentially excellent proton-conducting capacity. Fourier transform

© 2015 WILEY-VCH Verlag GmbH & Co. KGaA, Weinheim

infrared spectrum (FTIR) showed new bands between 800 and 1100 cm^{-1}, confirming again the successful introduction of HPW into EGO (Figure S2, Supporting Information). Considering the HPW concentration would directly influence the final loading amount, we soaked EGO monolith (50 mg) in HPW solution (10 mL) and methodically adjusted the solution concentration from 1 to 40 mg mL^{-1}. The loading of HPW raised with the increasing concentration and achieved equilibrium when the concentration exceed 25 mg mL^{-1} with a maximum loading amount of about 80 wt% (Figure S3, Supporting Information). Notably, even the HPW concentration was extremely low (1 mg mL^{-1}), the EGO monolith can still adsorb HPW from the solution completely and can hardly flush out, owing to the strong affinity between them. EDAX was also used to confirm the HPW content (Figure S4, Supporting Information), and the results were consistent with that calculated from UV–vis spectrum.

Another interesting phenomenon was observed in the post-treatment process. After oven-drying the PEGO and EGO monolith at 100 °C for 24 h, both of them experienced tremendous volume shrinkage of more than 90% (Figure S5, Supporting Information), which indicated huge empty space inside the monolith and thus well explained the record-breaking POMs loading capacity. However, when resoaked in the water, the two dried samples showed quite different responding. The volume of PEGO almost fully recovered in less than 4 h, by contrast there was no change for EGO even being soaked for more than 30 d (Figure S5, Supporting Information). The unique response to water of PEGO just like a bibulous sponge and provided visible solid evidence of its high hydrophilicity due to the introduction of POMs. We also explored the response effect of PEGO to other solvent, such as alcohol, acetonitrile, benzene, and methylbenzene. Similar volume restoring phenomenon was observed in alcohol and acetonitrile, but not in benzene and methylbenzene. We surmised that this effect could be attributed to the strong attraction between POMs and polar solvent molecules and the rigid pillaring of POMs which stabilized the interlayer space and avoided too closely stacking of adjacent nanosheets for solvent access.

In order to avoid the shrinkage during drying process, lyophilization was performed to maintain the monolith state. SEM images revealed the porous sponge-like inner structure in monolith PEGO and EGO (Figure 2). Agree with the volume shrinkage during soaking in HPW aqueous solution, the pore size of PEGO is obviously smaller than EGO. By contrast, there were no pores retained in the oven-dried samples because of the restacking of EGO and PEGO sheets (Figure S6, Supporting Information). The porous structure regained along with the volume recovery of PEGO (Figure S7, Supporting Information). Hence, the sponge-like response effect of PEGO to water can be attributed to the synergistic effect of hydrophilic POMs and cross-linking structure. Considering the extended diffusion path in monolith material, elemental mapping was carried out to determine the dispersion degree of HPW in the inner space of PEGO. The uniform dispersion states of W element proved highly decentralized HPW particles (Figure S8, Supporting Information), which can be attributed to the 3D interconnected channels providing accessible gallery for HPW diffusion.

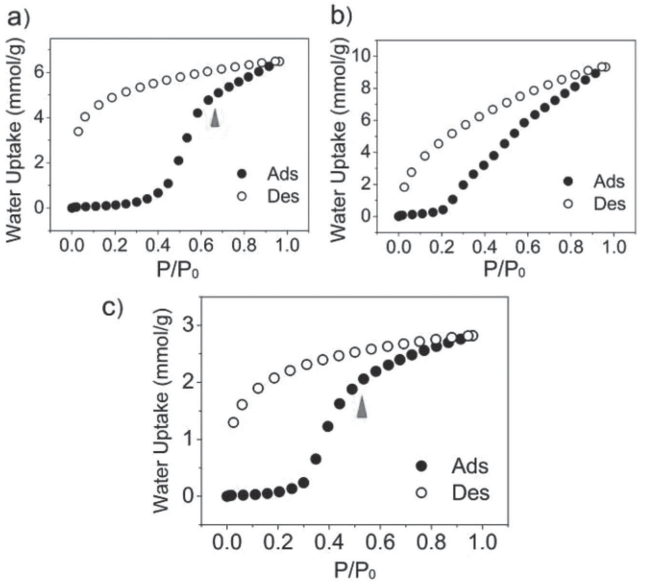

Figure 3. Water vapor adsorption isotherms of a) GO, b) EGO, and c) PEGO at 25 °C. The hysteresis loop of EGO was much smaller than that of GO and PEGO. The saturated adsorption point moved forward from about P/P_0 0.7 in GO to ≈0.5 in PEGO.

The proton diffusion in the interlayers of GO-based material depends on the formation and reformation of hydrogen bonds assisted by water molecules. Hence, the content of water would directly affect the proton conduction. To further assess the hydrophilicity of these hybrids, water vapor adsorption experiments were carried out. GO and PEGO both exhibited type-IV adsorption isotherm with large hysteresis loops demonstrating their high hydrophilic properties (**Figure 3**). EGO exhibited the worst hydrophilic ability proved from the smallest hysteresis loop (Figure 3b). This was also an explanation for the "sponge-like" behavior of PEGO mentioned before. However, what surprised us was the highest adsorption quantity of EGO, which might be derived from the lager interlamellar spacing pillared by EN molecules (Figure S9, Supporting Information). We tried to determine the interlayer space of EGO and PEGO by X-ray diffraction (XRD), but no diffraction peak was shown in the pattern, which might be attributed to the flexible nature of EN resulting in wrinkled construction and un-uniform distance between adjacent layers. Such result was also observed by other researchers.[27] Because of the filling of interlayer space by HPW units, the total adsorption amount of water in PEGO is the lowest comparing with GO and EGO. Considering the introduction of HPW increased the water retention of the material, which has been proved in metal-organic frameworks (MOFs) by us previously,[16] and only extremely low water content is necessary for the rapid exchange of protons between the Keggin-type units,[28] the low water content would not be a barrier for proton hopping in PEGO. More importantly, the saturated adsorption point shifted forward for PEGO comparing with GO, from about P/P_0 0.7 to 0.5 (Figure 3a,c). So, we deduced that a low RH (60% in this work) is adequate for PEGO to achieve a high conductivity.

Structural and component changes of EGO and PEGO, especially the amount of hopping sites, were determined by

© 2015 WILEY-VCH Verlag GmbH & Co. KGaA, Weinheim

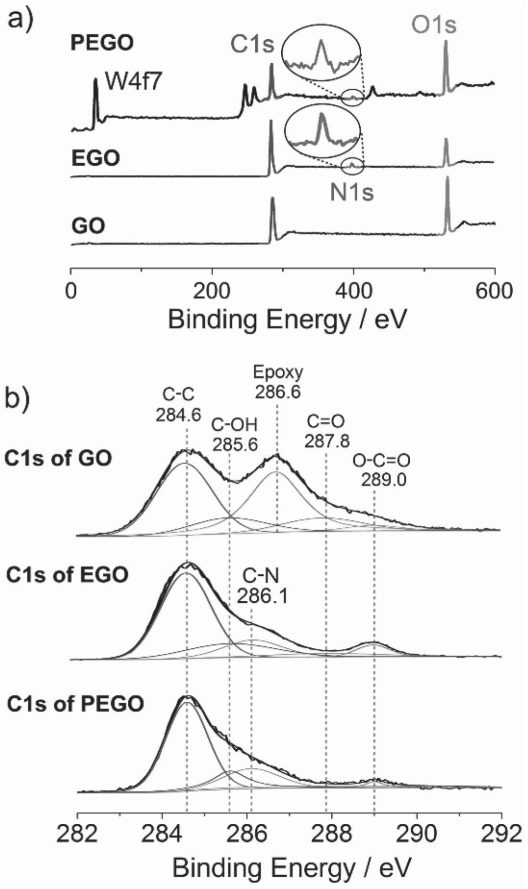

Figure 4. a) X-ray photoelectron spectra of GO, EGO, and PEGO; b) C1s spectrum of GO, EGO, and PEGO. There were epoxy, hydroxyl, and carboxyl groups on the basal plane of GO. The epoxy groups were totally reduced in EGO, and EN were grafted on the basal plane of GO proved by the appearance of C—N at 286.1 eV.

X-ray photoelectron spectroscopy (XPS). The amount of oxygen atoms experienced a fluctuation during the synthetic process, a decrease with the functionalization of EN followed by an increase with the introduction of HPW (**Figures 4** and S10, Supporting Information). Comparing with pristine GO, the peak of epoxy groups at 286.6 eV disappeared completely in EGO. Instead, the peak of C—N appeared at 286.1 eV indicated the replacement of unstable epoxy groups by EN. Hydroxyl and carboxyl groups were preserved in EN-functionalized GO. With the introduction of HPW, the total content of O atoms dramatically increased on account of abundant exterior oxygen atoms of Keggin units. However, there were no obvious changes in the C1s spectrum of PEGO comparing to that of EGO, indicating POMs were not bonded with the carbon atoms. It is worth noting that the final O/C ratio in PEGO was as high as of about 3/1. This value was 6–9 times higher than that in GO and EGO which were only 1/2 and 1/3, respectively, and implied much more continuous proton-conducting pathways in PEGO.

The proton conductivity of PEGO monolith with different HPW loading amount were measured by alternating current impedance spectroscopy. With the increase of HPW loading amount, the conduction gradually improved (Figure S11, Supporting Information). The monolithic PEGO loading 80 wt% HPW gave a proton conductivity of 2.4×10^{-3} S cm^{-1} at 25 °C and 60% RH (Figure S12, Supporting Information), which was one order of magnitude higher than GO nanosheets (≈10^{-4} S cm^{-1}) under the same condition.[5] The conductivity increased to 1.02×10^{-2} S cm^{-1} at 80 °C (Figure S13, Supporting Information) which was the highest under low RH among all GO-based materials. EGO gave an obviously lower conductivity value around 10^{-6} S cm^{-1} (Figure S14, Supporting Information). We proposed that the decrease in conductivity resulted from the high proton affinity of amino groups inhibiting protonic mobility. Similar phenomenon was also observed by Matsumoto and co-workers.[5] We further increased RH but no obvious improvement on proton conduction was obtained. This can be rationalized by the water adsorption saturation after 60% RH. To confirm the contribution of monolith state and sponge-like inner structure for proton transport, we also measure the pellet of powder samples obtained by oven-drying. The conductivity of PEGO pellet gave a proton conductivity of 8.4×10^{-4} S cm^{-1} at 25 °C and 60% RH (Figure S15, Supporting Information), which is only about one third of the monolith sample but was still comparable to GO nanosheets. We proposed that the obvious improvement in proton conduction are derived from the following factors: first, the insertion of POMs into the interlamination provided more mobile protons and flexible pathways. Protons can change path through hopping on the external oxygen atoms of Keggin units which could speed up transportation (**Figure 5**d). Second, the sponge-like cross-linking inner structure provided higher level of sheet-sheet connectivity (Figure 5b). Each hole wall can be seen as a multilayer nanosheet with thickness of several hundred nanometers (Figure 5c) which have been proved as ideal proton-conducting pathways dominated by in-plane transfer.[5] Third, the grain boundary resistance is eliminated in the monolithic status which is inevitable in pellet samples (Figure S16, Supporting Information). Finally, long-term tests were performed to evaluate the stability of PEGO. Owing to the replacement of epoxy groups by EN in PEGO and the high stability of POMs, the monolith PEGO sample operated for 1 month with little evidence of performance loss, but GO sample showed an obvious decrease (Figure S17, Supporting Information).

Driven by the curiosity about whether other inorganic acid has similar effectiveness for promoting proton transportation, we also measured the conductivities of EGO samples impregnated with sulfuric acid and phosphoric acid, respectively. In stark contrast to PEGO, there were no obvious reduction in volume for EGO monolith when soaked in neither sulfuric acid nor phosphoric acid aqueous solution (Figure S18, Supporting Information), and the "sponge-like" behaviors were not observed which might be due to the lack of pillaring effect owing to the much smaller sizes of the two anions (Figure S19, Supporting Information). Nevertheless, both of them showed high conductivities around 10^{-3} S cm^{-1} (2.94×10^{-3} S cm^{-1} for sulfuric acid and 0.82×10^{-3} S cm^{-1} for phosphoric acid at 25 °C and 60% RH, Figure S20, Supporting Information), which were in the same level with PEGO. Considering the corrosion of sulfuric acid and phosphoric acid to equipments, POMs would be a better choice for practical application.

© 2015 WILEY-VCH Verlag GmbH & Co. KGaA, Weinheim

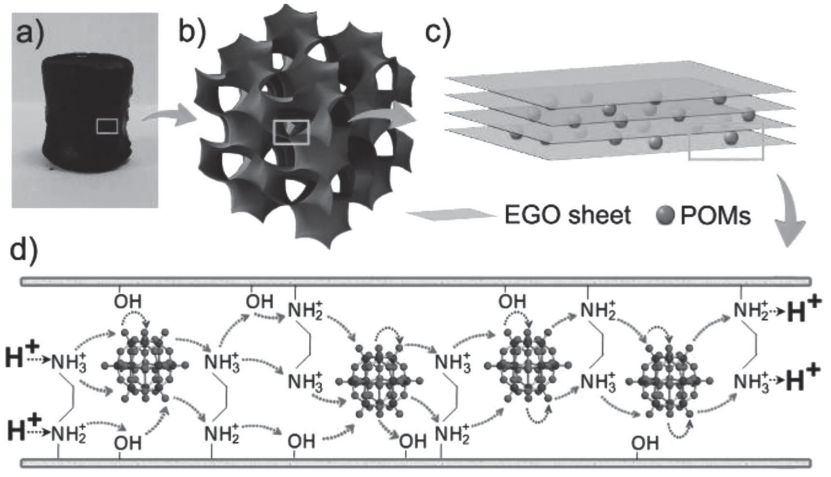

Figure 5. Proposed mechanism for proton conductivity in PEGO monolich. a) The optical photograph of PEGO monolich. b) The 3D corss-linking inner structure of the monolich sample.c) The pore walls can be seen as multilaminate nanosheets and d) there are multiple proton-conducting pathways in the interlayer space constructed by the external oxygen atoms and the hydroxyl and amino groups on the basal plane.

3. Conclusion

A high proton-conducting performance was achieved in polyoxometalate-modified GO monolith with 3D sponge-like inner structure under low relative humidity. The rapid proton diffusion originated from the in-plane protonic movement and the cross-linking of nanosheets in the molecular level mediated by EN and POMs. In addition, the introduction of POMs also provided abundant hopping sites and mobile protons which is a significant contribution to the rapid proton propagation. This research provided a practical way to access bulk in-plane proton conduction in GO-based materials, which has potential applications in fuel cells, electrochemical sensors and reactors.[29–33]

4. Experimental Section

Materials: All the raw chemicals were obtained commercially and used without additional purification.

Characterization: Fourier transform infrared spectroscopy (FTIR) were recorded in the range 400–4000 cm^{-1} on an Alpha Centaurt FTIR spectrophotometer using KBr pellets. Powder X-ray diffraction measurements were performed on a Rigaku D/MAX-3 instrument with Cu Kα radiation in the angular range 2θ 3°–60° at 293 K. Hidenisochema IGA 100B instrument was used to measure water vapor adsorption measurement at 293K. XPS were collected on Thermo ESCALAB 250X-ray photoelectron spectrometer. UV–vis spectrum was recorded on Mapada UV–vis-6100PC UV–vis spectrograph. Morphology analysis was performed by using a Quanta 250 FEG scanning electron microscope. EDAX spectrum was recorded by TEAM EDS (EDAX, USA) on HITACHI SU8010 SEM. AC impedance measurements of the samples were performed on a PARSTAT 2273 (AMETEK Instruments, USA) electrochemical workstation, the temperature and relative humidity are controlled by using an HDHWHS-50 incubator.

Synthesis of GO: Graphene oxide was prepared via a modified Hummers' method. Graphite powder (1.5 g), $NaNO_3$ (2.0 g) and concentrated H_2SO_4 (90 mL) was cooled to 0 °C by stirring in an ice bath for 15 min. 9.0 g $KMnO_4$ was added slowly with vigorous stirring while keeping the temperature below 5 °C. After an hour, the mixture was warmed to 35 °C for 30 min. Then 270 mL water was added slowly, the temperature rose gradually and was kept at 95 °C for another 30 min. Then 600 mL water was added. Finally, H_2O_2 (30%, 40 mL) was added to convert the unreacted permanganate and manganese dioxide into soluble sulfates. The mixture was centrifuged and the precipitate was washed with 5% HCl solution (one time) and then washed with water to neutral. The final precipitate was dried at 70 °C for 24 h. It was then dispersed in water (5 mg mL^{-1}) by 4 h sonication.

Synthesis of EGO: Ethylenediamine (EN, 0.2 mL) was added into graphene oxide dispersion (5 mg mL^{-1}, 10 mL). The mixture was sealed in a glass vessel and heated for 10 h at 90 °C for synthesis of EGO. After being washed with water, the monolith samples were lyophilized for 48 h. Powder samples were obtained by oven-drying the monolith at 100 °C for 24 h and then grind to powders.

Synthesis of PEGO: After EGO was obtained, the powder or monolith (50 mg) were soaked in HPW aqueous solution (10 mL) with different concentration (from 1 mg mL^{-1} to 40 mg mL^{-1}) for 4 h. The adsorption process was monitored by UV–vis spectrum and the adsorption amount was calculated from the concentration variation of HPW aqueous solution. Then the powder or monolith were washed with water for several times until the pH of filtrate was near 7. The final powders were dried at 100 °C for 24 h and the monolith samples were lyophilized for 48 h.

Synthesis of H_2SO_4 and H_3PO_4 Impregnated EGO: After EGO was obtained, the monolith was soaked in 100 × 10^{-3} M H_2SO_4 or H_3PO_4 aqueous solution for 4 h. Then the monolith was washed with water for several times until the pH of filtrate was near 7. The final monolith samples were oven-dried at 100 °C for 24 h or lyophilized for 48 h.

Supporting Information

Supporting Information is available from the Wiley Online Library or from the author.

Acknowledgements

This work was supported by the National Natural Science Foundation of China (Grant Nos. 21231002, 21371029, and 21171032), the Key Technologies R&D Program of Jilin Province of China (Grant No. 20130206079SF), and the Open Research Fund of the State Key Laboratory of Inorganic Synthesis and Preparative Chemistry (Jilin University, Grant No. 2015-01).

Received: May 10, 2015
Published online: June 16, 2015

[1] W. Gao, L. B. Alemany, L. Ci, P. M. Ajayan, *Nat. Chem.* **2009**, *1*, 403.
[2] D. A. Dikin, S. Stankovich, E. J. Zimney, R. D. Piner, G. H. B. Dommett, G. Evmenenko, S. T. Nguyen, R. S. Ruoff, *Nature* **2007**, *448*, 457.
[3] D. Li, M. B. Muller, S. Gilje, R. B. Kaner, G. G. Wallace, *Nat. Nanotechnol.* **2008**, *3*, 101.
[4] K. P. Loh, Q. Bao, G. Eda, M. Chhowalla, *Nat. Chem.* **2010**, *2*, 1015.
[5] K. Hatakeyama, M. R. Karim, C. Ogata, H. Tateishi, A. Funatsu, T. Taniguchi, M. Koinuma, S. Hayami, Y. Matsumoto, *Angew. Chem. Int. Ed.* **2014**, *53*, 6997.

© 2015 WILEY-VCH Verlag GmbH & Co. KGaA, Weinheim

[6] W. Gao, G. Wu, M. T. Janicke, D. A. Cullen, R. Mukundan, J. K. Baldwin, E. L. Brosha, C. Galande, P. M. Ajayan, K. L. More, A. M. Dattelbaum, P. Zelenay, *Angew. Chem. Int. Ed.* **2014**, *53*, 3588.
[7] M. R. Karim, K. Hatakeyama, T. Matsui, H. Takehira, T. Taniguchi, M. Koinuma, Y. Matsumoto, T. Akutagawa, T. Nakamura, S. Noro, T. Yamada, H. Kitagawa, S. Hayami, *J. Am. Chem. Soc.* **2013**, *135*, 8097.
[8] W. Gao, N. Singh, L. Song, Z. Liu, A. L. Reddy, L. Ci, R. Vajtai, Q. Zhang, B. Wei, P. M. Ajayan, *Nat. Nanotechnol.* **2011**, *6*, 496.
[9] S. Kim, S. Zhou, Y. Hu, M. Acik, Y. J. Chabal, C. Berger, W. de Heer, A. Bongiorno, E. Riedo, *Nat. Mater.* **2012**, *11*, 544.
[10] D. E. Katsoulis, *Chem. Rev.* **1998**, *98*, 359.
[11] I. V. Kozhevnikov, *Chem. Rev.* **1998**, *98*, 171.
[12] M. Yoon, K. Suh, S. Natarajan, K. Kim, *Angew. Chem. Int. Ed.* **2013**, *52*, 2688.
[13] O. Nakamura, T. Kodama, I. Ogino, Y. Miyake, *Chem. Lett.* **1979**, *8*, 17.
[14] E. Coronado, C. J. Gómez-García, *Chem. Rev.* **1998**, *98*, 273.
[15] Y. Zhou, J. Yang, H. Su, J. Zeng, S. P. Jiang, W. A. Goddard, *J. Am. Chem. Soc.* **2014**, *136*, 4954.
[16] Y. Liu, X. Yang, J. Miao, Q. Tang, S. Liu, Z. Shi, S. Liu, *Chem. Commun.* **2014**, *50*, 10023.
[17] S. Lu, D. Wang, S. P. Jiang, Y. Xiang, J. Lu, J. Zeng, *Adv. Mater.* **2010**, *22*, 971.
[18] T. Uma, M. Nogami, *Chem. Mater.* **2007**, *19*, 3604.
[19] H. Li, S. Pang, S. Wu, X. Feng, K. Mullen, C. Bubeck, *J. Am. Chem. Soc.* **2011**, *133*, 9423.
[20] D. Zhou, B.-H. Han, *Adv. Funct. Mater.* **2010**, *20*, 2717.
[21] H. Li, S. Pang, X. Feng, K. Muellen, C. Bubeck, *Chem. Commun.* **2010**, *46*, 6243.
[22] J. Chen, S. Liu, W. Feng, G. Zhang, F. Yang, *Phys. Chem. Chem. Phys.* **2013**, *15*, 5664.
[23] J.-P. Tessonnier, S. Goubert-Renaudin, S. Alia, Y. Yan, M. A. Barteau, *Langmuir* **2012**, *29*, 393.
[24] S. Wang, H. Li, S. Li, F. Liu, D. Wu, X. Feng, L. Wu, *Chem. Eur. J.* **2013**, *19*, 10895.
[25] D. R. Dreyer, S. Park, C. W. Bielawski, R. S. Ruoff, *Chem. Soc. Rev.* **2010**, *39*, 228.
[26] Y. Zhu, S. Murali, W. Cai, X. Li, J. W. Suk, J. R. Potts, R. S. Ruoff, *Adv. Mater.* **2010**, *22*, 3906.
[27] H. Hu, Z. Zhao, W. Wan, Y. Gogotsi, J. Qiu, *Adv. Mater.* **2013**, *25*, 2219.
[28] M. J. Janik, R. J. Davis, M. Neurock, *J. Am. Chem. Soc.* **2005**, 5238.
[29] K. D. Kreuer, S. J. Paddison, E. Spohr, M. Schuster, *Chem. Rev.* **2004**, *104*, 4637.
[30] D. R. Rolison, J. W. Long, J. C. Lytle, A. E. Fischer, C. P. Rhodes, T. M. McEvoy, M. E. Bourg, A. M. Lubers, *Chem. Soc. Rev.* **2009**, *38*, 226.
[31] L. Malavasi, C. A. J. Fisher, M. S. Islam, *Chem. Soc. Rev.* **2010**, *39*, 4370.
[32] K.-D. Kreuer, *Chem. Mater.* **1996**, *8*, 610.
[33] J. Peron, Z. Shi, S. Holdcroft, *Energy Environ. Sci.* **2011**, *4*, 1575.

© 2015 WILEY-VCH Verlag GmbH & Co. KGaA, Weinheim